RECENT PROGRESS IN MICROPLANE MODELLING OF PLAIN CONCRETE

FERHUN C. CANER[*] AND ZDENĚK P. BAŽANT[†]

[*] Instituto de Técnicas Energéticas (INTE)
Universidad Politécnica de Cataluña
Diagonal 647, 08028 Barcelona, Spain
e-mail: ferhun.caner@upc.edu

[†]Department of Civil and Environmental Engineering,
Northwestern University
2145 Sheridan Rd, Evanston, IL 60208, USA
e-mail: z-bazant@northwestern.edu

Key words: Concrete, Constitutive Modelling, Microplane, Fiber-reinforced, Finite Element Analysis

Abstract. Despite determined efforts in mathematical modelling of multiaxial behaviour of plain concrete by many researchers, the existing models have not achieved a full description of this complex behaviour. Among these models, the microplane models have contributed important advances in the semi-multiscale modelling of multiaxial behaviour of concrete since their inception in the early 80s. Among several versions of microplane models for plain concrete, model M4 had the greatest success in modelling both the rate-dependent dynamic and quasistatic multiaxial behaviours of concrete. Yet, some problems still have persisted, such as (1) a spurious lateral contraction under uniaxial tension, and (2) an unrealistic damage prediction in tension. These problems resulted from the difficulty in reconciling the pressure sensitive ductile behaviour in compression of concrete with its brittle tensile behaviour. A new microplane model, called M7 as a successor to the earlier microplane models for plain concrete, overcomes the aforementioned problems while retaining all of its compressive data fitting prowess. The volumetric-deviatoric split, required in the previous modelling of the pressure sensitive compressive behaviour of concrete, is now removed from the elastic strains under both compression and tension, but retained in the formulation of compressive stress-strain boundaries (i.e, strain-dependent yield limits on the generic microplane). This allows the simulation of a much more realistic tensile behaviour including the correct damage (loading/unloading slope) and correct lateral contraction. It also means that a new compressive normal boundary is needed. It is defined in terms of the existing deviatoric and volumetric boundaries, which preserves the versatility of the model in fitting a wide range of experimental data. Model M7 has been tested in finite element simulations of a wide range of compressive, tensile, mixed

938

mode fracture tests and vertex effect tests, as well as compression-tension load cycles. It has recently been extended to fiber reinforced concrete and rate dependent behaviour of plain concrete. Perforations of concrete walls by missiles in which enormous strain rates (on the order of 10^4s^{-1}) are encountered have also been simulated successfully using the rate dependent extension of the model M7, whose robustness is thus demonstrated.

1 INTRODUCTION

The idea that multiple yield surfaces must be active at any point of macroscopic continuum in the inelastic range of material response was proposed by G. I. Taylor as early as 1938 and later gave rise to "the slip theory" of plasticity, proposed by [1]. In this theory, projections of the stress tensor acted on slip planes. The shear strains on these planes, defined using the plasticity theory, were in turn assembled to form the plastic strain tensor. Using the additive separation of the total strain tensor into elastic and plastic parts, the total strain could be calculated from any prescribed stress tensor. This approach, broadly called the Taylor modelling, is arguably still the most efficient and accurate approach that describes the elastoplastic behavior of polycrystalline metals.

Concrete and other pressure sensitive quasibrittle materials, on the other hand, require the strain tensor to be prescribed to obtain a stable stress-strain response. Consequently, the strain tensor is projected over the potential failure planes, called the microplanes (to make reference to the fact that these planes are considered at a lower scale than the macroscopic continuum scale), instead of the stress tensor. The corresponding response of the material is evaluated over the microplanes by the prescribed vectorial stress-strain laws on the microplanes, and the resulting stress vectors are assembled to yield the macroscopic stress tensor using principle of virtual work.

Since 1983, a series of progressively improved microplane models labeled M0, M1, M2,...M6 have been developed for concrete, along with models M5f and M6f for inelastic behavior of short fiber reinforced concrete. The microplane framework was employed in modeling the constitutive behavior of many other engineering materials such as clays, soils, rocks, rigid foams, fiber composites (prepreg laminate and braided) and biological soft tissue as reviewed in detail in [2]. Among these models, model M4 may be considered a milestone for maximum data fitting capability. It features separation of microplane strains and stresses into volumetric and deviatoric parts and strain dependent yield limits that allow evaluation of microplane stresses given the microplane strains. However, model M4 has shortcomings in the modeling of tensile damage and lateral contraction under tension. Both of these shortcomings resulted from the inability to make the transition from pressure sensitive ductile failure in compression to brittle tensile failure. Both of the models M5 and M6 as well as the fiber-reinforced versions of these models M5f and M6f are attempts for a seamless continuous transition between these two extremes of concrete behavior. These models were successful in some finite element calculations, but later were

found to be problematic in large scale dynamic calculations, and therefore they were later deemed non-robust.

Model M7 [3, 4] solves this problem of seamless continuous transition from the pressure sensitive ductile behavior to brittle tensile behavior by removing the volumetric-deviatoric split of the elastic microplane normal strain while still retaining this split in inelastic strains. It removes the strain-dependent tensile deviatoric yield limit defined on the microplane, and defines a strain-dependent compressive normal yield limit as the sum of compressive volumetric and compressive deviatoric yield limits. Thus, model M7 retains the data fitting prowess of model M4 while providing a seamless transition from pressure-sensitive compressive behavior of concrete to brittle tensile behavior. This seamless transition allows, for the first time in the evolution of microplane modelling, a correct representation of both the tensile damage and the lateral contraction under tension. This is verified by numerous finite element simulations, including large-scale dynamic simulations, and is in addition to the capability to simulate pressure-sensitive compressive behavior of concrete with good accuracy.

Model M7 has been extended to simulation of the multiaxial behavior of short-fiber reinforced concrete, in a model labeled M7f [5]. The model M7f retains the prowess of the base model M7, and builds on it to include effects of various types of short fibers in both compression and tension. This model has also been verified against various experimental. Its robustness is ensured by the the robustness of M7 itself, the base model. In what follows, we briefly explain the fundamental relations behind the models M7 and M7f and demonstrate their data fitting capability using comparisons between the predictions and experimental data.

2   CONSTITUTIVE RELATIONS IN MODELS M7 AND M7F

The kinematic constraint in the microplane models for concrete is indispensable to capture the strain-softening behavior. It means that the microplane strains are the projections of the strain tensor on the microplanes [2, 7]:

$$\epsilon_N = n_i n_j \epsilon_{ij} = N_{ij} \epsilon_{ij} \tag{1}$$

in which n_i are the components of the unit normal vector of a generic microplane and $i, j = 1, 2, 3$ are the indices of the cartesian coordinate system (see Fig. 1 in [2]). The in-plane shear strain vector on each microplane is represented by its two in-plane orthogonal components in the directions of unit in-plane coordinate vectors $\vec{m}$ and $\vec{l}$ which are generated randomly on each microplane. Thus, the shear strains on the microplanes are defined as

$$\epsilon_M = \frac{1}{2} \left(n_i m_j + n_j m_i \right) \epsilon_{ij} = M_{ij} \epsilon_{ij}; \ \epsilon_L = \frac{1}{2} \left(n_i l_j + n_j l_i \right) \epsilon_{ij} = L_{ij} \epsilon_{ij} \tag{2}$$

To be able to model the pressure sensitive compressive behavior of concrete, it is necessary to split the microplane normal strain into its volumetric and deviatoric parts:

$$\epsilon_N = \epsilon_V + \epsilon_D; \ \sigma_N = \sigma_V + \sigma_D \tag{3}$$

where $\epsilon_V = \epsilon_{kk}/3$ and $\epsilon_D = (N_{ij} - \delta_{ij}/3)\epsilon_{ij}$. In model M7, this split is employed only in the modeling of compressive inelastic behavior.

The constitutive laws for compressive behavior of concrete on the microplane, expressed in terms of volumetric and deviatoric stresses σ_V and σ_D as well as the microplane shear stresses σ_M and σ_L, must be prescribed as functions of the corresponding microplane volumetric, deviatoric and shear strains. These generalized laws are given by: $\sigma_N^- = \sigma_V + \sigma_D$ where $\sigma_V = \mathcal{F}_V(\epsilon_V, \epsilon_I, \epsilon_{III})$ and $\sigma_D = \mathcal{F}_D(\epsilon_D, \epsilon_V)$; $\sigma_N^+ = \mathcal{F}_N(\epsilon_N, \sigma_V)$; and finally $\sigma_\tau = \mathcal{F}_T(\epsilon_L, \epsilon_V, \sigma_N)$ where $\tau = L, M$.

For computational robustness of the model, implicit equations that need to be solved by iterations are avoided. This means that the microplane constitutive laws should give the microplane stresses explicitly as far as possible. The explicitness has been achieved for the deviatoric and volumetric stresses on the microplanes. However, the friction law inevitably involves the normal stresses, which means it cannot be explicit.

2.1   Strain-dependent yield limits in models M7 and M7f

In what follows we briefly explain the microplane constitutive laws called the strain-dependent yield limits or simply the microplane stress-strain boundaries. Parameters that vary with fiber volume fraction are shown as functions of V_f.

The normal boundaries govern the tensile and compressive fracturing behavior (see Fig. 5a in [3]). For tensile fracturing,

$$
\begin{aligned}
\sigma_N^{b+} &= E k_1 \beta_1 e^{-\langle \epsilon_N - \beta_1 c_2 k_1 \rangle/(-c_4 \epsilon_e \, \mathrm{sgn}(\epsilon_e) + k_1 c_3)} \\
\text{where} \quad \beta_1 &= -c_1 + c_{17} e^{-c_{19}\langle \epsilon_e - c_{18}\rangle} + p_0(V_f)
\end{aligned}
\tag{4}
$$

For compressive behavior, the normal boundary is constructed as the sum of volumetric and deviatoric boundaries. For any state of stress, regardless of whether it is tensile or compressive, the normal stress is evaluated seamlessly using

$$
\sigma_N = \max[\min(\sigma_N^e, \ \sigma_N^{b+}), \ \sigma_N^{b-}] \text{ where } \sigma_N^{b-} = \sigma_V^b + \sigma_D^b
\tag{5}
$$

where σ_N^e is given in Eq. 17 and E_N is given in the first of Eqs. 13.

The deviatoric boundary simulates the spreading and splitting cracks under compression. It is given by (see Fig. 5b in [3]):

$$
\sigma_D^b = -\frac{E k_1 \beta_3}{1 + [\langle -\epsilon_D \rangle/(k_1 \beta_2)]^2}
\tag{6}
$$

$$
\text{where} \quad \beta_2 = c_5 \gamma_1 + c_7(V_f), \quad \beta_3 = c_6 \gamma_1 + c_8, \quad \gamma_0 = f_{c0}'/E_0 - f_c'/E
\tag{7}
$$

$$
\gamma_1 = e^{\gamma_0} \tanh(c_9 \langle -\epsilon_V \rangle/k_1)
\tag{8}
$$

The volumetric boundary simulates the pore collapse and expansive breakup of the

material. It is given by (see Fig. 5c in [3]):

$$\sigma_V^b = -Ek_1k_3e^{-\epsilon_V/k_1\alpha} \tag{9}$$

$$\text{where} \quad \alpha = \frac{k_5}{1+\epsilon_e}\left(\frac{\epsilon_I^o - \epsilon_{III}^o}{k_1}\right)^{c_{20}} + k_4 \tag{10}$$

in which k_i ($i = 1, 2, 3...$) are the adjustable scaling parameters whose numerical values will be discussed later; $\epsilon_I^o, \epsilon_{III}^o$ are the maximum and minimum principal strains at the beginning of the step; and $\epsilon_e = \langle -\sigma_V^o/E_{N0}\rangle$ (where $\langle x\rangle = \max(x,0) =$ Macauley brackets).

The frictional yield surface simulates the shear behavior of the model. It is given by (see Fig. 5d in [3]):

$$\sigma_T^b = F_T(-\sigma_N) = \frac{E_T k_1 k_2(V_f)c_{10}(V_f)\langle -\sigma_N + \sigma_N^0\rangle}{E_T k_1 k_2(V_f) + c_{10}(V_f)\langle -\sigma_N + \sigma_N^0\rangle} \tag{11}$$

where

$$\sigma_N^0 = \langle E_T k_1 c_{11}(V_f) - c_{12}(V_f)\langle \epsilon_V\rangle\rangle \tag{12}$$

2.2 Elastic behavior and damage

When the normal microplane strain ϵ_N is treated without splitting it into its volumetric and deviatoric parts, the microplane normal and shear stiffness constants E_N and E_T are given by (see Eq. 32 in [6]):

$$E_N = \frac{E}{1-2\nu}, \quad E_T = E_N\frac{1-4\nu}{1+\nu} \tag{13}$$

where $E =$ Young's modulus on the macrolevel and $\nu =$ Poisson's ratio (also $E_N = K/3$ where $K =$ bulk modulus). Obviously since both E_N and E_T must be non-negative, only Poisson's ratios in the range $\nu \in [-1, 0.25]$ can be reproduced.

This range of ν is sufficient for concrete, for which $\nu \approx 0.18$, but would not suffice for a general material with any thermodynamically admissible Poisson ratio $\nu \in [-1, 0.5]$. In that case, the microplane models M7 and M7f must both be coupled in series with an isotropic volumetric element of an infinite bulk modulus $K' = \infty$ but a finite shear modulus $G' \neq 0$ [7] (see Fig. 2 in [3, 5]). Using this series coupling, any thermodynamically admissible Poisson's ratio can be reproduced even when volumetric-deviatoric split of elastic strains is not employed.

The normal microplane elastic modulus evolves as follows:

$$\text{For } \sigma_N^0 \geq 0: \quad E_N = E_{N0}e^{-c_{13}\epsilon_N^{0+}}f(\zeta) \tag{14}$$

$$\text{but } E_N = E_{N0} \text{ if } \sigma_N^0 > E_{N0}\epsilon_N \text{ and } \sigma_N^0\Delta\epsilon_N < 0 \tag{15}$$

$$\text{For } \sigma_N^0 < 0: \quad E_N = E_{N0}\left(e^{-c_{14}|\epsilon_N^{0-}|/(1+c_{15}\epsilon_e)} + c_{16}\epsilon_e\right) \tag{16}$$

In Eq.14, $f(\zeta) = (1 + a\zeta^2)^{-1}$ in which $\zeta = \int < d\epsilon_V >$ and typically $a = 0.1$ has been employed to extend the validity of the model to many load cycles and has virtually no effect for the first few cycles [8].

The elastic normal microplane stress is given by:

$$\sigma_N^e = \sigma_N^0 + E_N \Delta\epsilon_N \tag{17}$$

When unloading occurs on the microplanes with normals in the direction of the maximum principal tensile strain, the response will inevitably intersect the initial elastic loading path. This is due to the damage (or degradation) of the elastic stiffness. The condition in Eq. 15 makes sure that, after the intersection, the unloading follows the initial elastic slope towards the origin, instead of continuing to proceed along the original unloading path even after the intersection. Following the original unloading path after the two paths have intersected would be incorrect because it would cause negative dissipation during load cycles.

2.3 Effect of the short fibers

For mode I cracks, the contribution of a fiber to the crack-bridging stress is assumed to be given by a simplified form of Kholmyansky's equation [9]:

$$\sigma_N^f = \begin{cases} E p_1 k_1 \langle \epsilon_N/k_1 \rangle e^{-p_2 \langle \epsilon_N/k_1 \rangle} & \text{if } \epsilon_N/k_1 < 1/p_2 + p_4 \\ E p_1 k_1/p_2 e^{-1} & \text{if } 1/p_2 + p_4 \leq \epsilon_N/k_1 < p_3 \\ E p_1 k_1 \langle \epsilon_N/k_1 - p_3 + 1/p_2 \rangle e^{-p_2 \langle \epsilon_N/k_1 - p_3 + 1/p_2 \rangle} & \text{if } p_3 \leq \epsilon_N/k_1 \end{cases} \tag{18}$$

This law results from gradual activation of fibers bridging an opened crack as shown in Fig 5. of [5]. Obviously, the fiber and the matrix are assumed to be coupled in parallel, resulting in a microplane normal stress given by

$$\sigma_N^{bf+} = \sigma_N^{b+} + \sigma_N^f \tag{19}$$

where σ_N^{bf+} = total tensile normal boundary for fiber reinforced concrete, σ_N^{b+} = tensile boundary for plain concrete matrix and σ_N^f =contribution of the fiber given by Eq.18.

In the presence of fibers, to calculate the microplane normal stresses σ_N, Eq.5 is modified by replacing the σ_N^{b+} by σ_N^{bf+}:

$$\sigma_N = \max[\min(\sigma_N^e, \sigma_N^{bf+}), \sigma_N^{bf-}] \tag{20}$$

in which $\sigma_N^{bf-} = \sigma_V^{bf} + \sigma_D^{bf}$, σ_N^e is given in Eq. 17 and E_N is given in the first of Eqs. 13. The microplane shear stresses and stress increments are given by

$$\begin{aligned} \sigma_\tau &= \min(|\sigma_\tau^e|, \sigma_\tau^b) \\ \Delta\sigma_M &= E_T \Delta\epsilon_M \frac{\sigma_\tau}{\sigma_\tau^e} \\ \Delta\sigma_L &= E_T \Delta\epsilon_L \frac{\sigma_\tau}{\sigma_\tau^e} \end{aligned} \tag{21}$$

where $\sigma_\tau^e = \sqrt{(\sigma_M^0 + E_T \Delta \epsilon_M)^2 + (\sigma_L^0 + E_T \Delta \epsilon_L)^2}$, $\sigma_M = \sigma_M^0 + \Delta \sigma_M$, $\sigma_L = \sigma_L^0 + \Delta \sigma_L$ and E_T is given by the second of Eqs.13. Finally the micro-macro stress equilibrium is enforced by

$$\sigma_{ij} \;=\; \frac{3}{2\pi} \int_\Omega \left[\sigma_N N_{ij} + \sigma_M M_{ij} + \sigma_L L_{ij} \right] d\Omega \tag{22}$$

The typical parameter values for the fixed "c" parameters and those for the free "k" parameters of the model M7 as well as the "p" parameters of the model M7f are given in Tables 1 through 8 in [5] for fiber reinforced concrete data fits. For plain concrete data fits, the "k" and "c" parameters are given in [4].

2.4   Thermodynamic Dissipation

Thermodynamically sound constitutive models must obviously satisfy the condition that the density of dissipation rate must be non-negative. In microplane models, this criterion could easily be satisfied by requiring the dissipation rate on each microplane to be non-negative. However, there are two problems with such a simple requirement:

- The dissipation rate on each microplane being nonnegative is only a sufficient condition, not a necessary one; only the dissipation rate on all the microplanes combined must be nonnegative, which means that it can be negative on some.

- Purely elastic unloading is not realistic, and so the effect of damage due to material stiffness loss must be known. Depending on the unloading path, energy can be, and is, dissipated or released.

This distinction between the enforcement of positive dissipation on the microplane level and on the macroscopic continuum level is important because the former reduces the data fitting capability of these models. A more detailed discussion of the difficulties in enforcing a nonnegative thermodynamic dissipation is given in [3].

3   RESULTS AND DISCUSSION

The first problem in which model M7 is tested is the loading with uniaxial compression-tension cycles reaching the strength limit for uniaxial tension. Fig. 1 shows such cycles simulated by model M7 as the solid curves superposed on the dashed curves representing the test data reported in [10]. The specimen analyzed and the finite element mesh are shown in the inset figure. The specimen is a concrete cylinder with a circumferential notch 5 mm deep and 5 mm wide. The gauge length, which is 25 mm, is taken as the length of the whole cylinder, to simplify the finite element analysis. The diameter of the cylinder is 120mm. The max. aggregate size of the concrete was 16mm. The necessity of a localization limiter is satisfied by carrying out the analysis according to the crack band model. During the simulations, it is observed that the crack localizes in the plane

of the notch. Clearly, the discrepancy between the test data and the simulation is quite small and is appreciable only in the transition from tension to compression. The predicted response is perfectly continuous.

The next test problem for the verification of the model M7 is the simulation of the test data designated in [11] as "Type 2". In this test, a much higher shear stress in the crack-tip cross section is achieved by controlling the displacement at the free end of the beam, whose dimensions are the same as in the aforementioned mixed-mode test. Here the machine stiffness, which may be imagined to be simulated by the spring controlling the displacement of the free end, is of utmost importance. For example, if the machine stiffness is assumed to be infinite, the beam does not fail by a crack emanating from the notch tip, but rather by a new crack that develops in the tension zone at the left support. But if the machine has a finite stiffness, equivalent to a spring stiffness of approximately $K = 3000$ N/mm acting at point B (see the inset figure shown in Fig.2b), then a crack emanating from the notch tip is obtained in the simulations. In Fig. 2a, the experimentally observed crack pattern is superimposed on the finite element mesh in which the crack appears in various shades. The darker the shade, the more open the crack is. Clearly, the experimental and predicted cracks coincide. Fig. 2b compares the load versus the crack mouth opening displacement measured in the test to that predicted by model M7. The predicted response is in excellent agreement with the measured response. For a more detailed calibration and verification of the model M7, see [4].

The M7f predictions of some of the experimental data for concrete reinforced with PVA fibers subjected to uniaxial tension are shown in Fig.3 [12]. Clearly the fits for different fiber volume fractions are good. Fig. 4 [13] shows the biaxial failure envelope for different fiber volume fractions. The predictions by model M7f are quite accurate. For a more detailed calibration and verification of model M7f, see [5].

4   CONCLUSIONS

Recently, a new microplane model for multiaxial behavior of concrete, called model M7, has been developed. It can accurately simulate tensile damage, tension/compression load cycles and lateral contraction in both tension and compression, in addition to pressure-sensitive compressive behavior of concrete. Model M7 has been extended to predict the multiaxial behavior of the short fiber reinforced concrete, to yield a model labeled M7f.

The advantages of M7, which transcend to M7f as well, are briefly as follows: 1) The volumetric-deviatoric split is avoided for the elastic strains and is applied only to the stress-strain boundaries; 2) as a consequence, the excessive lateral strains and stress locking in far post-peak extension are eliminated and it becomes possible to reproduce the differences between hydrostatic compression and uniaxial compression under rigid lateral confinement, as well as the high shear dilatancy of low strength concretes; and 3) the unloading, reloading and load cycles can be captured realistically, even if they cross between tension and compression, etc.; in detail, see [3, 4].

The effect of fibers in compressive response of lower strength concretes is made depen-

dent on the fiber volume fraction and the plain concrete model is recovered when this fraction vanishes. The fiber resistance is a function of the strain representing the average opening of cracks of given spacing. Compared to previous models, introduced is a new refined model in which the fibers bridging the crack and resisting its opening are considered to be in different regimes, some fibers already softening and others still hardening (see Fig 5 in [5]). A fiber law of the same form is systematically used to fit all the test data. The parameters of this law depend on the fiber volume fraction and the fiber type.
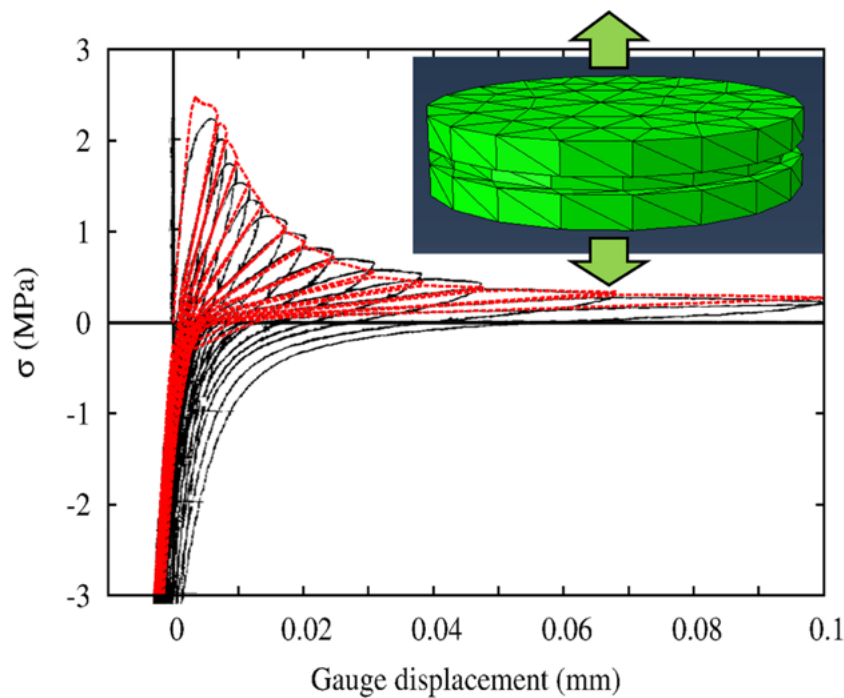

Figure 1: Finite element simulations of compression-tension load cycles in which test data are by [10]

REFERENCES

[1] Batdorf, S. and Budianski, B. A mathematical theory of plasticity based on the concept of slip.*Technical Note 1871, Nat. Advisory Committee for Aeronautics, Washington, D.C.* (1949).

[2] Bažant, Z. P., Caner, F. C., Carol, I., Adley, M. D. and Akers, S. A. Microplane model M4 for concrete: I. Formulation with work-conjugate deviatoric stress. *Journal of Engineering Mechanics, ASCE* (2000) **126**(9):944–953.

[3] Caner, F. C. and Bažant, Z. P. Microplane model M7 for plain concrete:I. Formulation. *J. of Engineering Mechanics, ASCE* (2013) doi:10.1061/(ASCE)EM.1943-7889.0000570.

[4] Caner, F. C. and Bažant, Z. P. Microplane model M7 for plain concrete:II. Calibration and verification. *J. of Engineering Mechanics, ASCE* (2013) doi:10.1061/(ASCE)EM.1943-7889.0000571.

[5] Caner, F. C., Bažant, Z. P. and Wendner, R. Microplane model M7f for fiber reinforced concrete. *Engineering Fracture Mechanics* (2013) **105**:41–57.

[6] Carol, I. and Bažant, Z. P. Damage and plasticity in microplane theory. *International Journal of Solids and Structures* (1997) **34**(29):3807–3835.

[7] Bažant, Z. P. and Oh, B.-H. Microplane model for progressive fracture of concrete and rock. *Journal of Engineering Mechanics, ASCE* (1985) **111**:559–582.

[8] Kirane, K. and Bažant, Z. P. Modification of the normal boundary in microplane model M7 to simulate Paris Law type fatigue. Private communication. (2013).

[9] Kholmyansky, M. M. Mechanical resistance of steel fiber reinforced concrete to axial load. *Journal of Materials in Civil Engineering* (2002) **144**:311–319.

[10] Reinhardt, H. W. and Cornelissen, H. A. W. Post-peak cyclic behavior of concrete in uniaxial tensile and alternating tensile and compressive loading.*Cement and Concrete Research* (1984) **14**(2):263–270.

[11] Gálvez, J., Elices, M., Guinea, G., and Planas, J. Mixed mode fracture of concrete under proportional and nonproportional loading.*International Journal of Fracture* (1998) **94**:267–284.

[12] Li, Z., Li, F., Chang, T.-Y.-P., and Mai, Y.-W. Uniaxial tensile behavior of concrete reinforced with randomly distributed short fibers. *ACI Materials Journal* (1998) **95**(5):564–574.

[13] Yin, W. S., Su, E. C. M., Mansur, M. A., Hsu, T. T. C. Biaxial tests of plain and fiber concrete. *ACI Materials Journal* (1989) **86**(3):236–243.
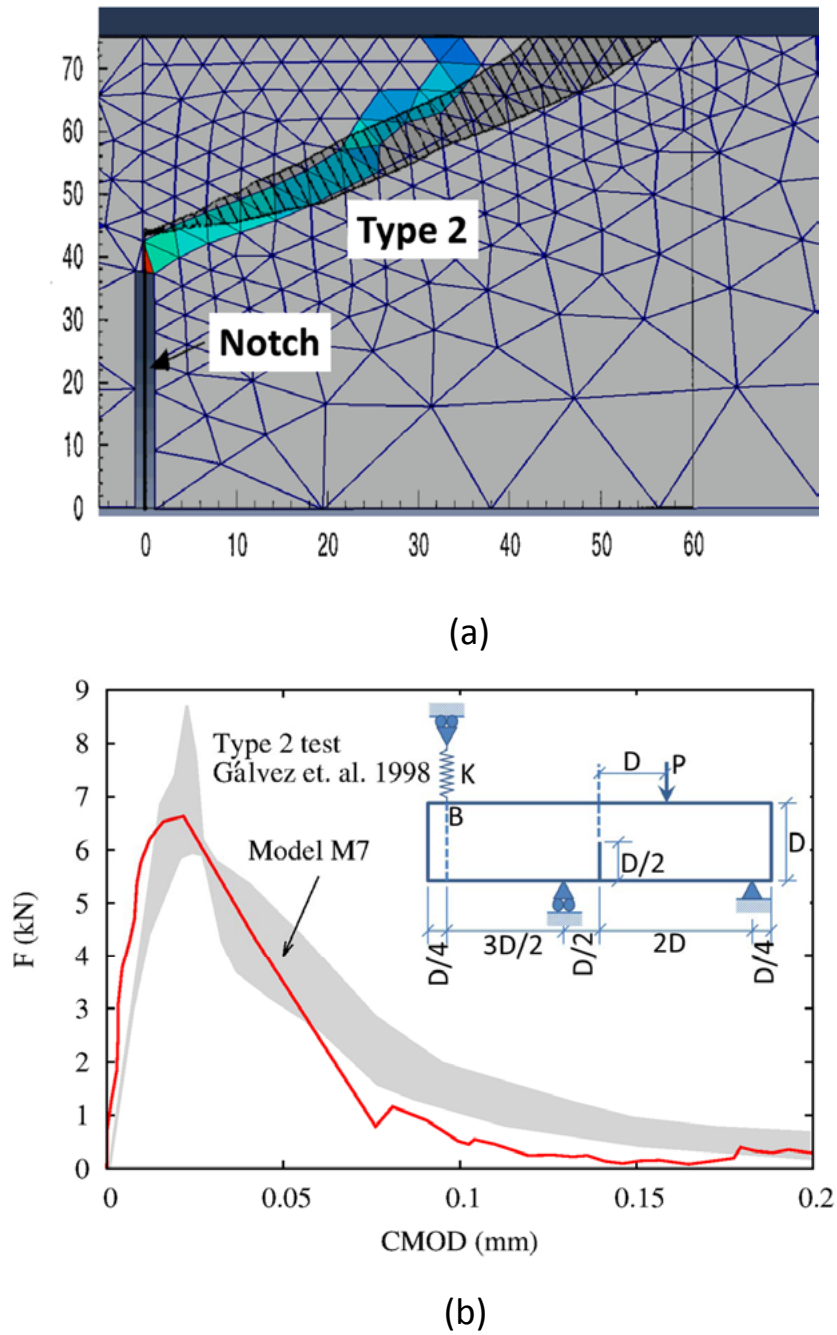
(a)

(b)

Figure 2: Finite element simulation of crack propagation and failure of asymmetrically notched three-point bend beam, with the displacement at a fourth point controlled to remain zero during the test. (a) Simulated and measured crack patterns, (b) simulated and measured load vs crack mouth opening displacement (CMOD). The test data and the inset figure of the test setup are by [11].
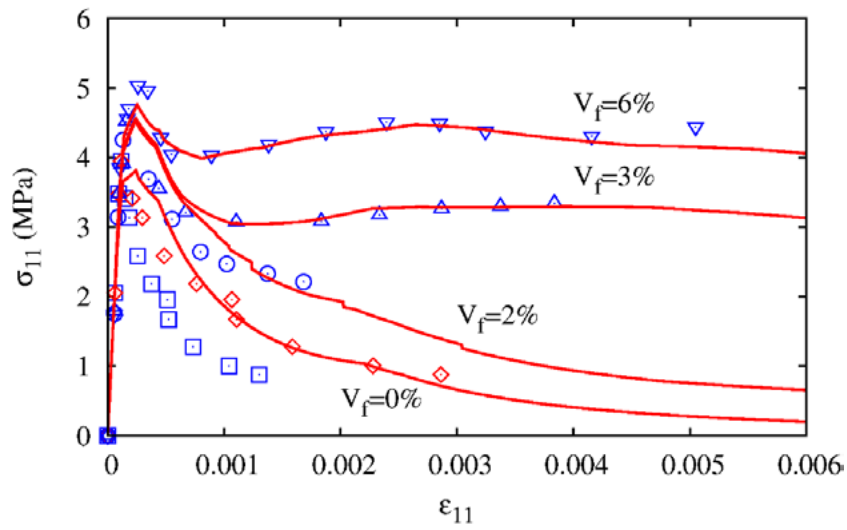
Figure 3: Uniaxial tensile test data for FRC with $V_f = 2, 3$ and 6% of PVA fibers [12] and their simulation by the model M7f. The data for plain concrete under uniaxial tension is also shown for comparison.
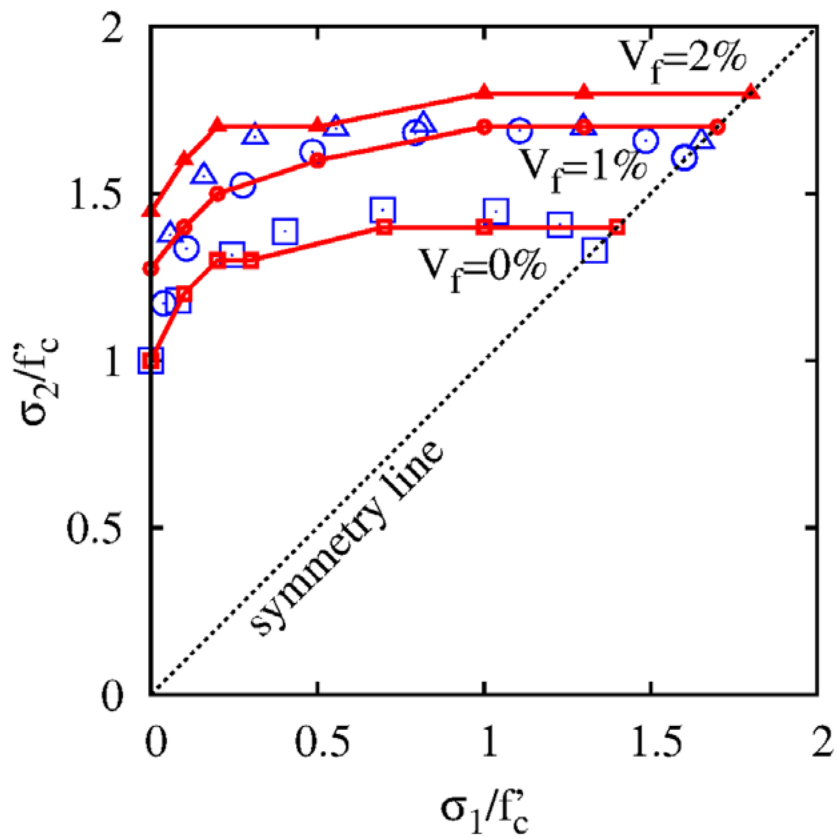

Figure 4: Biaxial compression test data for FRC with $V_f = 0, 1$ and 2% of steel fibers [13] and their simulation by the model M7f.